Multifunctional $Ti_3C_2T_x$ MXene Composite Hydrogels with Strain Sensitivity toward Absorption-Dominated Electromagnetic-Interference Shielding

Yunyi Zhu, Ji Liu,* Tong Guo, Jing Jing Wang, Xiuzhi Tang, and Valeria Nicolosi*

ABSTRACT: The fast development of terahertz technologies demands high-performance electromagnetic interference (EMI) shielding materials to create safe electromagnetic environments. Despite tremendous breakthroughs in achieving superb shielding efficiency (SE), conventional shielding materials have high reflectivity and cannot be re-edited or recycled once formed, resulting in detrimental secondary electromagnetic pollution and poor adaptability. Herein, a hydrogel-type shielding material incorporating MXene and poly(acrylic acid) is fabricated through a biomineralization-inspired assembly route. The composite hydrogel exhibits excellent stretchability and recyclability, favorable shape adaptability and adhesiveness, and fast self-healing capability, demonstrating great application flexibility and reliability. More interestingly, the shielding performance of the hydrogel shows absorption-dominated feature due to the combination of the porous structure, moderate conductivity, and internal water-rich environment. High EMI SE of 45.3 dB and broad effective absorption bandwidth (0.2−2.0 THz) with excellent refection loss of 23.2 dB can be simultaneously achieved in an extremely thin hydrogel (0.13 mm). Furthermore, such hydrogel demonstrates sensitive deformation responses and can be used as an on-skin sensor. This work provides not only an alternative strategy for designing next-generation EMI shielding material but also a highly efficient and convenient method for fabricating MXene composite on macroscopic scales.

KEYWORDS: MXene, composite, multifunctional hydrogel, electromagnetic interference shielding, terahertz absorption

Terahertz radiation with unique properties has been mainly focused on increasing electrical conductivity,[10,12−19] long studied and stimulated the rapid development of which is favorable for reducing thickness but would result in terahertz technologies in various fields, such as severe reflection and detrimental secondary electromagnetic communication,[1,2] biological sensing,[3] imaging,[4] and security pollution. To reduce the reflection of a shielding material, detection.[5,6] As a result, electromagnetic interference (EMI) optimized impedance matching is required to allow the shielding materials toward terahertz radiation are highly entrance of radiation into the shield.[20,21] Then the penetrated required to eliminate the radiation leaks and create safe electromagnetic wave should be attenuated to ensure high EMI electromagnetic environments, especially in terahertz circuits SE (Figure S1). Unfortunately, the conductive properties and and quasi-optical systems, ensuring that the delicate electronic impedance matching are mutually incompatible.[22−25] High devices can work properly.[7,8] In particular, the shielding electrical conductivity that ensures sufficient conductive loss materials should possess flexibility, minimal thickness, and high and attenuation capability would cause impedance mismatch shielding efficiency (SE) to meet the increasingly stringent requirements. Generally, the key to obtaining high EMI SE lies in minimized radiation transmission by either reflecting or

Received: October 22, 2020
Accepted: December 30, 2020
Published: January 5, 2021

attenuating the incident waves.[9,10] Carbon materials, such as carbon nanotubes and graphene, and their composites were the material of choice for terahertz EMI shielding due to the low densities and high conductivities.[11] However, previous efforts to design high-performance EMI shielding materials were

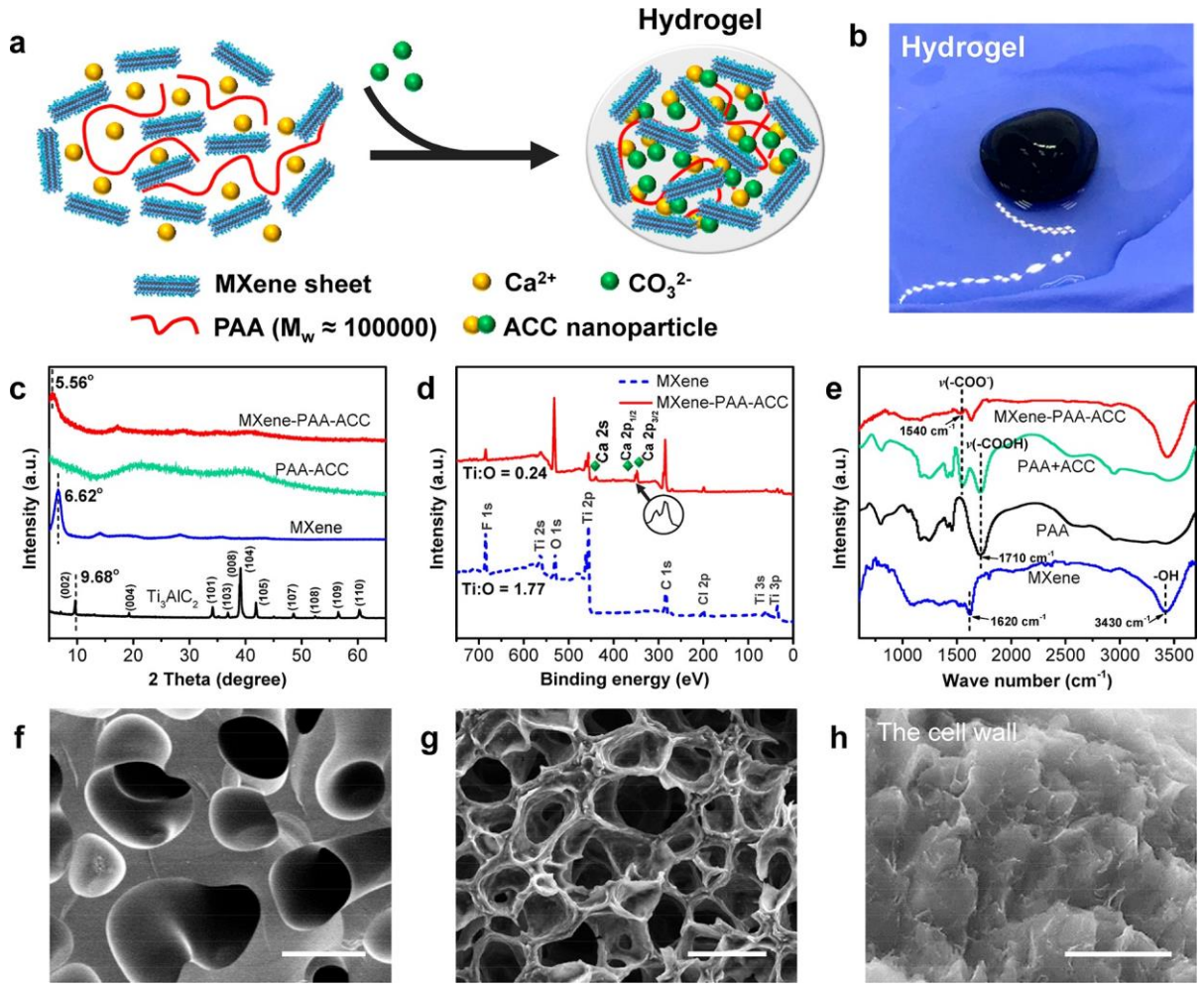

Figure 1. Fabrication and structural characterization of the MXene composite hydrogel. (a) Schematic illustrating the formation of MXene composite hydrogel. (b) Photograph of an as-synthesized MXene composite hydrogel. (c) XRD, (d) XPS survey, and (e) FT-IR spectra of MXene composite hydrogel and the reference samples. SEM images of (f) PAA-ACC hydrogel and (g, h) MXene composite hydrogel. Scale bars: (f) 20 μm, (g) 20 μm, (h) 2 μm.

and strong reflection character whereas low conductivity that ensures minimized reflection leads to insufficient radiation dissipation and poor shielding performance. Designing porous structures can relieve the conflict by interrupting the conducting networks and promoting internal reflection and scattering.[26−32] However, the large thickness is needed to allow efficient attenuation of the penetrated wave due to the reduction of conductivity.[8,33] To the best of our knowledge, there is no report on realizing efficient EMI shielding with negligible reflection in an ultrathin shielding material. In addition, once fabricated, conventional shielding materials exhibit fixed shapes and cannot be re-edited and recycled or recover from damage, impeding the application flexibility and reliability. Therefore, to confront these challenges, a pioneering alternative strategy for developing next-generation highperformance shielding materials beyond the usual design strategies is urgently needed to meet the escalating demands of the increasing complexity of modern devices and service environments.

Water has been widely demonstrated to be capable of generating polarization loss and attenuating electromagnetic waves in both gigahertz and terahertz bands.[34−38] It can be inferred that if enough water molecules could be immobilized in a material with moderate conductive properties, enhanced attenuation of the penetrated waves can be achieved without inducing unnecessary reflection. Hydrogel is a class of engineering materials constructed of a network of cross-linked hydrophilic building blocks surrounded by water,[39] showing potential for providing absorption-dominated EMI shielding performance. Furthermore, in striking contrast to dry materials, soft polymer hydrogels can deliver stunning arbitrarily shapechanging and self-healing abilities, ensuring the formation of conformal and stable interfaces with the sheltered objects, holding great promise in wearable electronics.[39−42] Nevertheless, such polymer hydrogels are typically nonconductive, leading to insufficient EMI shielding capability. Therefore, a key process for developing hydrogel-type EMI shielding materials is to engineer approaches to achieve moderate conductivity while retaining the unique properties and internal water-rich environment. Recently, newly emerged two-dimensional (2D) transition metal carbides and/or nitrides, named as MXenes, have shown great potential for EMI shielding.[10,43−49] The metallic electrical conductivity combined with rich surface chemistry makes MXene productive for constructing conductive

networks in composites and providing considerable conductive and polarization losses.[50] To this day, various macroscopic MXene composite materials were fabricated for a wide range of applications.[51−54] However, MXene composite hydrogels for EMI shielding applications have not been explored so far.

Herein, we demonstrate a strategy that assembles $Ti_3C_2T_x$ MXene sheets through a biomineralization-inspired assembly method to fabricate a hydrogel-type shielding material with a hybrid structure consisting of MXene, poly(acrylic acid) (PAA), and amorphous calcium carbonate (ACC) (MXenePAA-ACC). The as-prepared MXene composite hydrogel exhibits moderate conductivity, excellent stretchability and recyclability, favorable shape adaptability and adhesiveness to various surfaces, and fast self-healing capability, making it multifunctional with great application flexibility and reliability. More importantly, benefiting from the combination of porous structure, moderate conductivity derived from the MXene network, and internal water-rich environment, the hydrogel shows an absorption-dominated EMI shielding behavior. A high EMI SE of 45.3 dB, an excellent refection loss (RL) of 23.2 dB, and a broad effective absorption bandwidth (EAB, 0.2−2.0 THz) can be simultaneously achieved in an extremely thin hydrogel (0.13 mm). Furthermore, the sensing characteristics of the multifunctional hydrogel are also investigated.

RESULTS AND DISCUSSION

The MXene composite hydrogel was synthesized through a biomineralization-inspired assembly process as schematically illustrated in Figure 1a, b.[40,55] $Ti_3C_2T_x$ MXene nanosheets were first synthesized through selectively chemical etching the Al layers of the Ti_3AlC_2 powders followed by sonicationassisted exfoliation (Figure S2).[56] Their ultrathin and geometric features were observed by scanning electron microscopy (SEM) and atomic force microscopy (AFM) (Figure S3). The X-ray diffraction (XRD) pattern of the exfoliated $Ti_3C_2T_x$ shows a sharp (002) peak at $2\theta = 6.62°$, which corresponds to an enlarged interlayer distance of 1.33 nm as compared with that observed in the Ti_3AlC_2 (0.91 nm), and no diffraction peaks of Ti_3AlC_2 were detected (Figure 1c). These results confirmed the successful exfoliation of $Ti_3C_2T_x$ nanosheets.

To obtain MXene composite hydrogels, typically, the $Ti_3C_2T_x$ MXene suspension was mixed with PAA and $CaCl_2$ under vigorous stirring to form a stable mixture. Then, the Na_2CO_3 solution was added carefully using a pipet until a sticky precipitate gradually formed (Figure S4). It can be inferred that the MXene nanosheets were fully integrated into the hydrogel as the solution became almost clear after the fabrication process (Figure S4). All the composite hydrogels with varying weight percent of MXene to PAA (6.5, 8.5, 10.0, and 12.2 wt %) were fabricated by using the same protocol and are termed as 6.5, 8.5, 10.0, and 12.2 wt % MXene-PAA-ACC, respectively (Table S1). An excess of MXene would lead to poor structural integrity (Figure S5). Note that this text will principally refer to the 8.5 wt % MXene-PAA-ACC that exhibits optimized properties. The XRD results confirm that the d-spacing increased to 1.59 nm for MXene-PAA-ACC from 1.33 nm for pristine MXene, indicating that the PAA chains and ACC have been intercalated between MXene sheets (Figure 1c). The broad diffraction scattering could be due to the formation of localized regions where the periodicity of MXene layers is disturbed by the insertion of PAA chains.[57] The X-ray photoelectron spectroscopy (XPS) was employed to reveal the chemical composition (Figure 1d). In the XPS survey spectra, the MXene-PAA-ACC shows much stronger C and O signals than pristine MXene, indicating that abundant oxygen-containing groups on the PAA chains are introduced, which is crucial for providing cross-linking sites in the hydrogel. The overlap between Ti 2p peaks in MXene alone and MXene-PAA-ACC further indicates that the MXene is well protected from oxidation during the fabrication process (Figure S6), which is consistent with the XRD data. The formation of ACC was confirmed by the appearance of peaks of Ca 2p at 347.6 and 351.0 eV in the XPS spectrum, and the peaks corresponded to the lattice frequency and the symmetric stretching of the carbonate ion in the Raman spectra (Figures 1d and S7). Besides, no other crystalline peaks can be observed in the XRD pattern, identifying the amorphous phase of PAA and ACC. The component of the composite hydrogel was further confirmed by thermal gravimetric analysis (TGA) (Figure S8). Fourier-transform infrared (FT-IR) spectroscopy was performed to provide more detailed information for elucidating the cross-linking structure (Figure 1e). From the spectrum of MXene, mainly peaks assigned to −OH groups were observed. As for the pristine PAA, the peak at 1710 cm^{-1} could be assigned to the −COOH group. In the spectrum of MXene-PAA-ACC, the peak assigned to −OH shifted to 1640 cm^{-1} and a new peak at 1540 cm^{-1} ($-COO^-$) was observed, indicating the formation of hydrogen bonding and the chelation between $-COO^-$ and Ca^{2+}.[40,55]

Based on the above analysis, a cross-linking mechanism can be speculated. During the fabrication process, the negatively charged $Ti_3C_2T_x$ MXene sheets were first slightly flocculated in the presence of PAA chains and divalent cations (Ca^{2+}) by hydrogen bonding and electrostatic interaction. With the addition of CO_3^{2-}, ACC nanoparticles were formed to physically cross-link the PAA chains and $Ti_3C_2T_x$ sheets, which push the mixture past the phase boundary.[55] Finally, an integrated MXene composite hydrogel can be gradually formed. Thus, synergistic interactions occurred in the hydrogel to form a hierarchically cross-linking structure. The SEM images on the cross-section reveal the homogeneous and porous nature of the hydrogels (Figure 1f−h). As compared with the pure PAA hydrogel (PAA-ACC) that exhibits smooth fracture morphology (Figure 1f), the MXene composite hydrogel shows the rough surface of the cracked cell walls (Figure 1g), in which the overlapped MXene sheets with a layered structure can be observed (Figure 1h). In addition, the MXene composite hydrogel exhibits a smaller pore size and thinner cellular wall, leading to higher pore density (Figures S9, S10). The porous structure combined with the hydrophilic nature of MXene and PAA finally ensures a

water-rich environment inside the composite hydrogel (Figure S11).

The rheology properties are investigated by dynamic mechanical measurements. As shown in Figure S12a, the dynamic modulus (G′) is very close to, or even lower, than the loss modulus (G″) in the low-frequency range for the PAAACC, indicating the liquid-like behaviors (Figure S13). Adding MXene nanosheets can effectively strengthen the hydrogel and results in a solid-like behavior, as verified by the G′/G″ value that exceeds 1 in the whole frequency range 0.1−10 Hz (Figure S12a). Note that the G′ increased slightly with frequency, reflecting the existence of the physical cross-links in the hydrogel.[58] In addition, the MXene-PAA-ACC exhibits a high initial viscosity (~10^4 Pa·s) and an obvious shear-thinning behavior (Figure S12b). These rheology properties indicate that the MXene composite hydrogel can be pinched into arbitrary shapes to conform to different surfaces, representing a significant advantage over other solid materials that cannot be re-edited once fabricated.

before breaking. The superb stretchability is attributed to the high water content and the numerous hydrogen bonding, which can provide space for the solid components to reorient and break to dissipate the stress during the deformation process, respectively.[59] The rheology behaviors further endow the hydrogel with excellent processability (Figure 2b, c). As shown in Figure 2c, the hydrogel serves as ink for extrusion printing and can be smoothly extruded from a nozzle to form complex shapes, offering an attractive opportunity for satisfying the demanding design rules and large-scale applications. More importantly, due to the soft, sticky, and malleable features, the composite hydrogel can conformally adhere to objects with complex 3D geometry and can keep intact during deformation, demonstrating its significant advantage as compared with conventional solid EMI shielding materials, such as MXene films that possess superb shielding performance but very limited adaptability to deformation (Figure 2d−f).

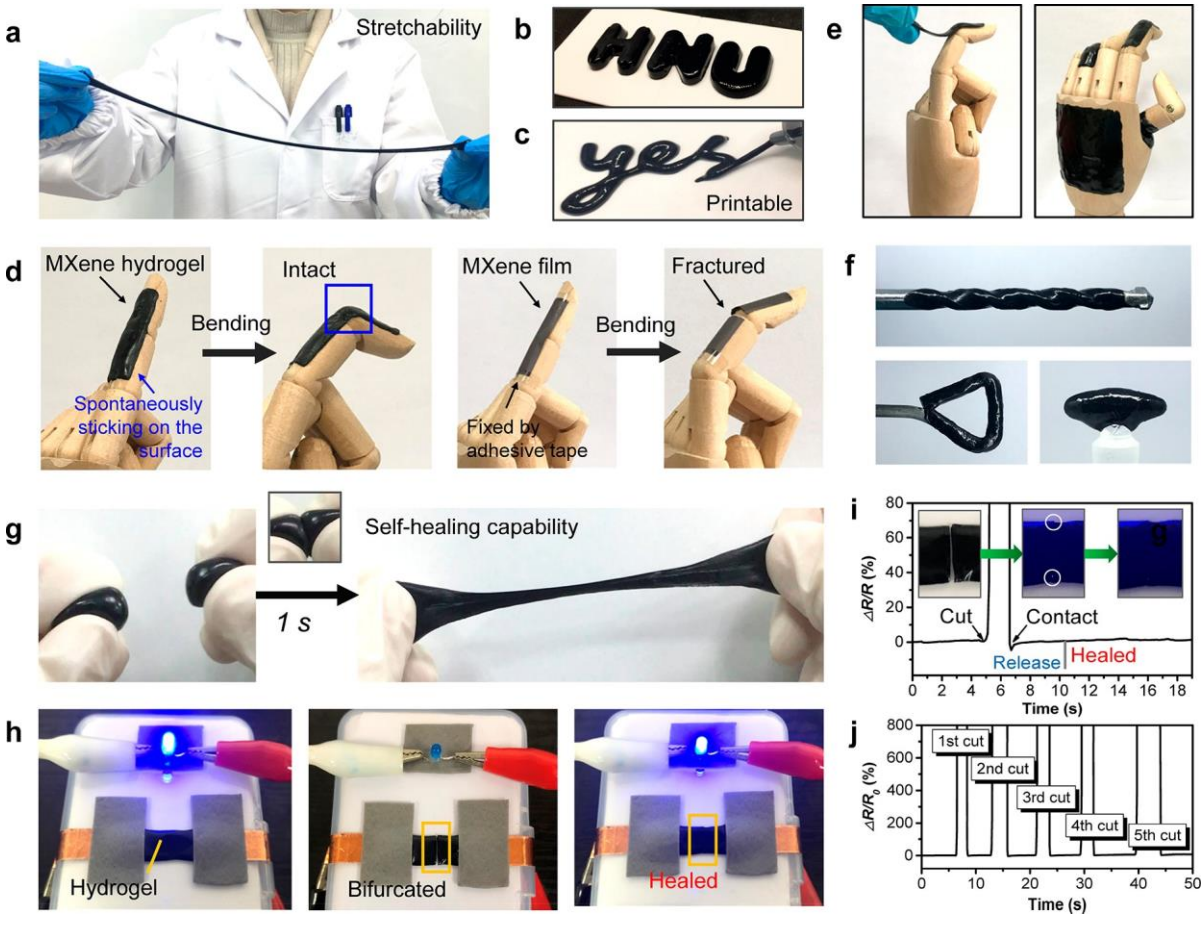

Figure 2. Photographs showing the (a) stretchability, (b, c) processability, (d−f) shape adaptability and adhesiveness, and (g, h) fast selfhealing capability of the MXene composite hydrogel. (i) The variation of resistance during a cutting−healing process under ambient conditions. (j) Cycling of the cutting−healing processes.

The MXene composite hydrogel possesses many interesting features. For instance, the hydrogel is highly stretchable and malleable. As shown in Figures 2a and S14, a piece of the hydrogel can be repeatedly stretched into a fiber-like material with a stretchability over 1500% strain

Self-healing ability that can significantly extend the service life and make the material more reliable for practical applications is another useful function for high-performance EMI shielding materials. Herein, the rapid and reproducible self-healing ability of the hydrogel is demonstrated in Figure 2g–j. Once two pieces of the hydrogel are gently attached, the interface can be healed instantaneously at ambient conditions without any further assistance and the healed hydrogel still demonstrates good stretchability (Figures 2g, S14–S16, and Movie S1). Figure 2h presents a circuit composed of a LED bulb and a piece of MXene composite hydrogel as the conductor. The LED bulb can be fully lighted when a large driving voltage (18 V) was applied, indicating the moderate conductivity of the hydrogel. Then the hydrogel was cut and separated into two halves and the LED bulb extinguished. Finally, when the two separated hydrogels were attached, the LED bulb immediately glowed again. To further investigate the self-healing property, the resistance change during the healing process was recorded. As shown in Figure 2i, the resistance increased to infinity immediately once the hydrogel was cut off and then returned to the original value in a very short time as the two separated parts were attached, indicating the complete recovery of the hydrogel. Even though the cutting and healing processes were repeated a few times, the resistance is still stable and similar to the initial value, demonstrating the stable selfhealing performance (Figure 2j). The self-healing property should be originated from the rich functional groups on PAA chains and MXene sheets, which provide abundant sites for forming interfacial hydrogen bonds with each other and crosslinking interactions with calcium ions during the healing process.[55,60] The composite hydrogels can be solidified by drying to form rigid composites (Figure S17). The dried samples can be readily converted into hydrogels by swelling in water, and the self-healing ability and flexibility could be well retained even after few drying-swelling cycles (Figure S18). It is worth mentioning that the self-healing process of dried samples can also be triggered by moisture, during which the damage can be healed by dropping water on the fractured surfaces to allow swelling and then putting them together for a while (Figure S19). Therefore, the MXene composite hydrogel with desirable shape-changing and fast self-healing ability can adapt to arbitrary complex surfaces and recover from serious damage quickly, guaranteeing its reliability as a high-performance EMI shielding material for applications in complex environments.

To explore the EMI shielding performance of the MXene composite hydrogel, the electrical properties are studied first. Figure 3a shows the dependence of electrical conductivity on the MXene content. The conductivity slightly increases with the MXene content but is maintained in a low range from 0.1

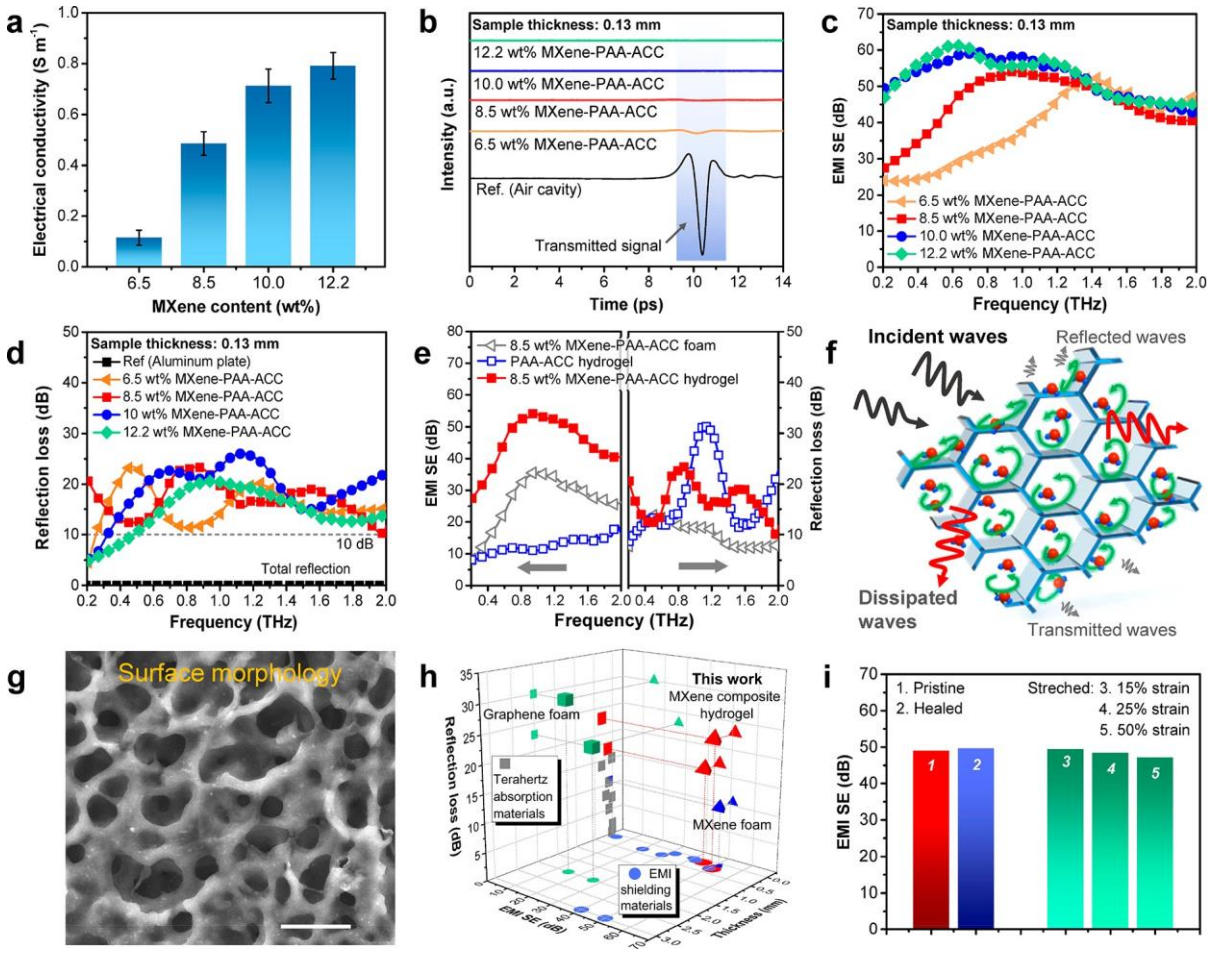

Figure 3. Absorption-dominated terahertz EMI shielding performance. (a) Electrical conductivity of MXene composite hydrogels. (b) THzTDS spectra and (c) EMI SE of MXene composite hydrogels. (d) RL curves of MXene composite hydrogels. (e) Comparison of terahertz EMI shielding and absorption performances between MXene composite hydrogel and reference samples. (f) Proposed absorptiondominated EMI shielding mechanism of the MXene composite hydrogel. (g) SEM image showing the surface morphology of the MXene composite hydrogel. (h) Comparison of the terahertz shielding and absorption performances. (i) Terahertz EMI shielding performances of a MXene composite hydrogel (0.29 mm) at different states. Scale bar: (g) 10 μm.

to 0.8 S m^{-1}. The moderate conductive property could play a key role in ensuring the optimized impedance matching while maintaining considerable attenuation capability (Figure S1).[22,23] The terahertz EMI shielding performance in the frequency range 0.2−2.0 THz was measured by terahertz timedomain spectroscopy (THz-TDS) at transmission mode (Figure S20a). The terahertz time-domain spectra show that the transmitted terahertz radiation intensities of the MXene composite hydrogels are much smaller than that of the incident wave and become almost undetectable when MXene content exceeds 8.5 wt %, qualitatively demonstrating that the incident terahertz electromagnetic waves are almost fully shielded (Figure 3b). The corresponding average EMI SE values are 38.6, 45.3, 52.4, and 52.8 dB for 6.5, 8.5, 10.0, and 12.2 wt % MXene composite hydrogels, respectively.

The reflection behaviors of the hydrogels were explored by a THz-TDS system at reflection mode (Figure S20b). In this mode, the hydrogel is with its back surface against an aluminum plate, which can almost fully reflect the radiation. Generally, two main reflection signals including the reflected signal from the surface of samples (I_{R1}) and the signal reflected by aluminum plate (I_{R2}) could be detected for materials with a large thickness due to the significant difference in the transmission distance of I_{R1} and I_{R2}.[61] As shown in Figure S21, the peaks of I_{R1} and I_{R2} merged due to the extremely small thickness of the samples. The intensities of reflected signals from the composite hydrogels are much smaller than that from the aluminum plate, demonstrating the minimized surface reflection and the effective wave dissipation inside the hydrogels. Figure 3d shows the RL curves of MXene composite hydrogels. All of the samples exhibit superior radiationabsorbing features in the measured frequency range. For the 8.5 wt % MXene-PAA-ACC with a small thickness of 0.13 mm, the maximum RL value (RL_{MAX}) reaches 23.2 dB and the EAB is 1.8 THz, which fully covers the measured frequency range. Excessive MXene inevitably increases more reflection, which can enhance the EMI SE but compromises the absorption performance.

To further ascertain the shielding mechanism, the terahertz EMI shielding and absorption performances of the MXene composite hydrogel and foam and the pure PAA-ACC hydrogel are compared, respectively (Figure 3e). The PAAACC hydrogel is insulating, but it still shows a moderate EMI SE value of 12.6 dB and strong electromagnetic absorption capability (RL_{MAX} = 31.3 dB, EAB = 1.75 THz), confirming the positive effect of water in dissipating the penetrated wave. For the MXene composite hydrogel, its average RL value slightly decreased due to the formation of conductive MXene network, which inevitably leads to higher surface reflection. However, with the addition of MXene, a much higher EMI SE of 45.3 dB can be achieved because the increased conductive and polarization losses derived from the MXene network contribute to the enhanced attenuation of the penetrated wave at the same

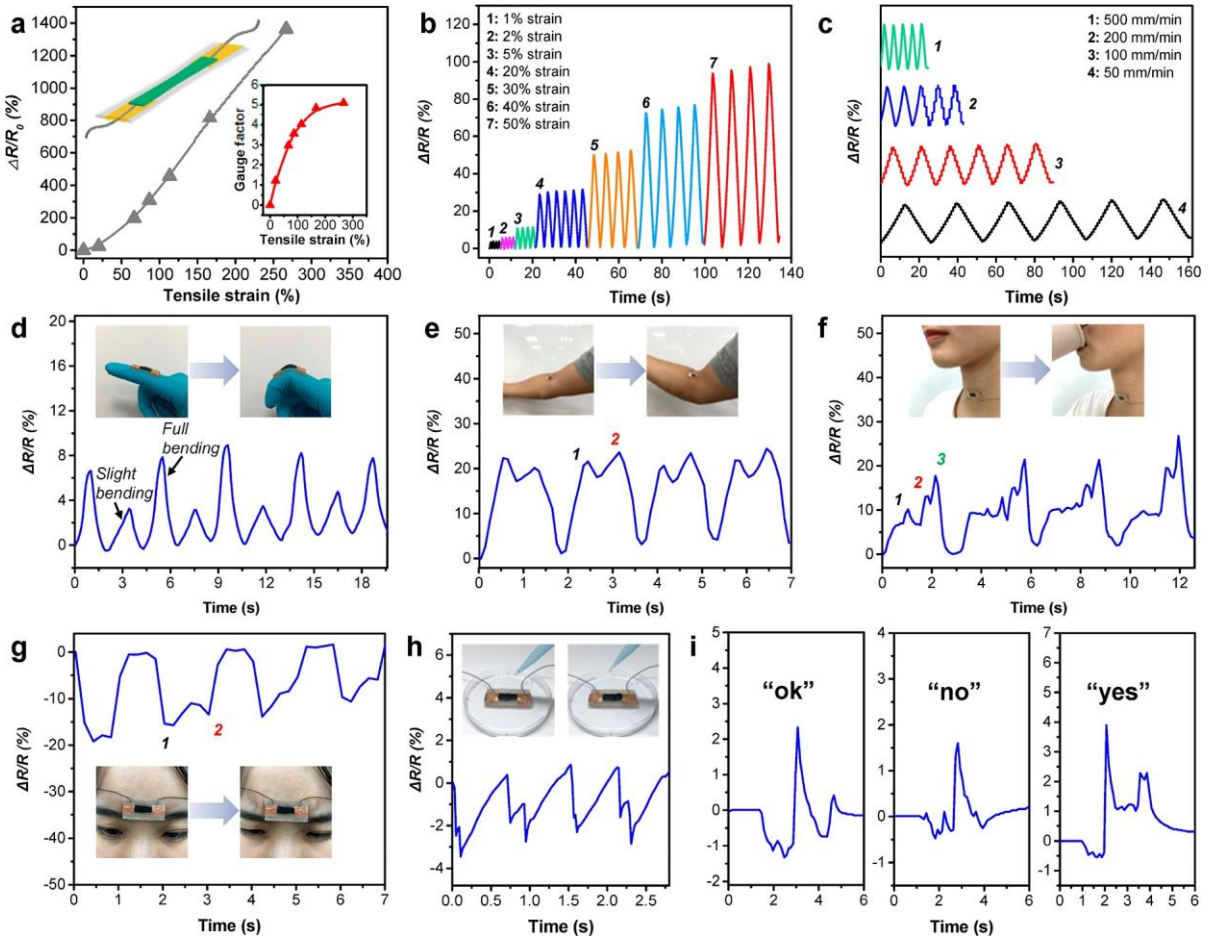

Figure 4. (a) Normalized electrical resistance versus stretch for the sensor. (b) Normalized resistance changes of the sensor under different tensile deformation. (c) Normalized resistance changes of the sensor under the strain of 50% with different deformation frequencies. Resistance changes of the sensor in response to different body movements: (d) finger bending, (e) arm bending, (f) swallow, and (g) frown. Resistance changes in response to (h) water droplet and (i) signature on the sensor.

time, which also agrees well with the dielectric constants (Figure S22). Note that the corresponding freezedried MXene composite foam possesses both poor shielding and absorption performances. Therefore, the synergistic effect of conductive MXene network and internal water-rich environment should play a key role in efficiently shielding the incident electromagnetic wave with minimized reflection.

Based on the above results, we can speculate an absorptiondominated EMI shielding mechanism, as schematically illustrated in Figure 3f. First, the electromagnetic wave can enter the hydrogel without significant reflection due to the surface open porous structure (Figure 3g) and the moderate conductivity that ensure the optimized impedance matching.[23,30] Then the penetrated wave propagated in the cells of the hydrogel and was repeatedly scattered and reflected by the conductive cell walls, which can extend the path length of the wave and enhance its interaction with the interfaces before transmission.[22,43] The surface terminations on the MXene sheets and the significant mismatch of conductivity in the interfaces between MXene and PAA can also effectively increase polarization losses to promote the attenuation of the penetrated wave.[43,62] Last but not least, the penetrated radiation energy would concentrate in the water area that is capable of providing both strong polarization loss and dielectric loss, and vortex-like current loops can be induced to further dissipate the electromagnetic energy.[38,63] Note that thicker samples have stronger EMI shielding capability while maintaining desirable absorption performance (Figure S23). Thus, with the absorption-dominated EMI shielding feature, our MXene hydrogel is ranked at the top of the comparison chart, showing its distinct advantage as compared with both the terahertz EMI shielding materials and the terahertz absorption materials reported so far (Figure 3h and Table S2). More interestingly, the terahertz EMI shielding performance can be well maintained even after repeated cutting-healing and stretching processes, demonstrating the reliability of the composite hydrogel to be applied in flexible devices (Figures 3i and S24).

In addition to providing absorption-dominated electromagnetic protection functions, the MXene composite hydrogel also shows electromechanical responses to deformation and can be used as a sensor for perceiving body motions and digitally monitoring vital signals, which is highly needed for wearable smart electronics.[64,65] Here, a sensor was fabricated by using elastomeric VHB tape as the substrate to encapsulate the hydrogel. As shown in Figure 4a, the electrical resistance of the sensor monotonically increases with the increasing strain under uniaxial stretch. Note that the resistance increased slowly in the initial strain range, which ensures that the EMI shielding performances would not be significantly affected when deformation is caused by the movement of the sheltered objects. The resistance response of the sensor was measured by applying different cyclic tensile strains and stretching rates (Figure 4b, c). The sensor can detect minor deformation with a strain of only 1% and the resistance change can reach stable state even at high stretching rates of 500 mm min^{-1}, demonstrating the reliability of the sensor. The sensor was further used to detect body movements. As shown in Figure 4d, e, the response behaviors of the sensor were recorded when the finger and arm were repeatedly bent. The sensor can respond to the movements repeatedly and detect the bending angles. In addition, more complex and subtle body movements, such as swallow and frown, can be successfully detected by mounting the sensor on the neck and forehead, respectively (Figure 4f, g). Both of the movements can yield distinct response behaviors, and the resistance signals are fully recoverable and repeatable. Note that the hydrogel with adhesiveness can also be used as an on-skin sensor by directly adhering to any positions on the human body (Figure S25). Moreover, the sensor presents pressure-sensing properties and can be used for recognizing signatures, further demonstrating the multifunctionality of our MXene composite hydrogels for applications in various scenarios (Figure 4h, i). Therefore, with the combination of these advantageous attributes, the MXene composite hydrogel holds great potential for application in the next-generation electronics beyond the conventional EMI shielding materials.

CONCLUSIONS

In summary, we have developed a multifunctional MXene composite hydrogel with excellent stretchability and recyclability, favorable shape adaptability and adhesiveness, fast selfhealing ability, and sensing capability to provide efficient terahertz EMI shielding. The synergy among the moderate conductivity, porous structure, and internal water-rich environment renders the hydrogel with absorption-dominated EMI shielding performance. The EMI SE of a 0.13 mm thick hydrogel reaches 45.3 dB with an RL_{MAX} value of 23.2 dB and a broad EAB covering the full measured frequency range (0.2− 2.0 THz), outperforming that of other terahertz shielding and absorption materials reported so far. Moreover, the hydrogeltype shielding material can conformally adhere to objects with arbitrarily complex geometry and quickly recover from damage, showing great promise for applications in wearable electronics and artificial skin. Accordingly, we believe this work can provide an alternative strategy for designing next-generation terahertz EMI shielding materials and a highly efficient and convenient method for developing multifunctional 3D MXene structure on macroscopic scales, which will significantly extend the applications of MXene materials.

METHODS

Synthesis of MXene. $Ti_3C_2T_x$ MXene was synthesized by a chemical etching method as reported.[56] Typically, 1.6 g of lithium fluoride (Aladdin) was mixed with 20 mL of 9 M hydrochloric acid under stirring in a Teflon bottle. Then, 1 g of Ti_3AlC_2 powder (average particle size ≤38 μm) was added into the above-mentioned solution and the mixture was stirred at 35 °C for 24 h. After the etching reaction, the products were washed with deionized water repeatedly until the pH value of the supernatant is higher than 5. Finally, the etched products were mildly sonicated under inert gas flow followed by centrifuging to remove impurities and obtain a

delaminated $Ti_3C_2T_x$ MXene suspension. To measure the conductivity of the MXene, the MXene suspension was vacuum-filtrated to obtain a freestanding MXene film, which showed a conductivity of 2000 S/cm.

Fabrication of MXene Composite Hydrogels and PAA Hydrogel. In a typical procedure, 266.6 mg of $CaCl_2$ were dissolved in 6 mL of 0.4 M PAA solution ($M_w \approx 100\ 000$ g mol^{-1}, SigmaAldrich) to obtain a PAA/$CaCl_2$ solution. Subsequently, the PAA/ $CaCl_2$ solution and MXene suspension (4 mg mL^{-1}) were mixed with different volume ratios under magnetic stirring for 30 min. Then a solution of 0.1 M Na_2CO_3 was slowly injected into the mixture while the mixture was vigorously stirred. During the process of adding Na_2CO_3 solution, flocculation can be observed and the sticky precipitates gradually accumulated around the stirring bar to form an integrated composite hydrogel. Finally, the composite hydrogel was collected and washed with deionized water. To fabricate the PAA hydrogel, the Na_2CO_3 solution was slowly injected into the solution of 0.4 M PAA and 0.4 M $CaCl_2$ under vigorous stirring and the asformed white precipitate was collected and washed. The volume of MXene, PAA/$CaCl_2$, and Na_2CO_3 solutions used to fabricate samples with different MXene content is listed in Table S1.

Characterization. The microstructures of the freeze-dried hydrogel were observed using a TESCAN MIRA SEM. The morphologies and geometric features of MXene sheets were confirmed by Bruker AFM. XRD data were collected with a Bruker D8 Advance XRD (Cu Kα radiation, λ = 1.54 Å). Chemical compositions of samples were confirmed with a Thermo Fisher Escalab 250 XPS and a Nicolet Nexus 670 FT-IR spectrometer. The rheological properties were measured by an AR2000ex rheometer. The electrical property was measured by an RTS-8 four-probe resistivity meter. The resistance signals were recorded in a CHI660E electrochemical workstation. The mechanical property was tested by a Xiangjie XJ830 universal testing machine. Raman analysis was performed on a Renishaw InVia Raman microscope. TGA was performed on a NETZSCH TGA209F1 at a rate of 10 °C min^{-1} under a nitrogen atmosphere.

Terahertz Shielding and Absorption Measurements. The terahertz EMI shielding performance and the reflection behaviors were obtained using THz-TDS at transmission mode and reflection mode, respectively. The measurements were performed at room temperature. The humidity in the test room was controlled in a low range (<5%). The terahertz pulse was generated using a GaAs photoconductive antenna with a Ti:sapphire laser as the excitation source. The terahertz signals were detected by a silicon-on-sapphire photoconductive antenna. The EMI SE values were calculated using the following equation:[8]

$$\text{EMI SE} = -20 \log(E_s/E_a) \quad (1)$$

where E_s and E_a refer to the amplitudes of transmission terahertz pulses for the samples and the air cavity, respectively.

The RL values of the samples were calculated according to the following equation:[61]

$$\text{RL(dB)} = -10 \log(E_r/E_i) \quad (2)$$

where E_r and E_i refer to the amplitude of the reflection signal of the samples and the amplitude of the incident terahertz pulse, respectively.

ASSOCIATED CONTENT

* Supporting Information

The Supporting Information is available free of charge at https://pubs.acs.org/doi/10.1021/acsnano.0c08830.

Basic characterization of $Ti_3C_2T_x$ MXene nanosheets and MXene composite hydrogels; supplementary XPS, Raman, and TGA data; SEM and AFM images of samples; photographs of samples; rheology measurements and mechanical assessments of samples; schematics of EMI shielding and self-healing mechanisms; supplementary terahertz EMI shielding and absorption performances; supplementary sensing performance; comparison of terahertz EMI shielding and absorption performance (PDF)

Movie S1: The fast self-healing capability and stretchability of the MXene composite hydrogel (MP4)

AUTHOR INFORMATION

Corresponding Authors

Ji Liu − College of Materials Science and Engineering, Hunan University, Changsha, Hunan 410082, China; Centre for Research on Adaptive Nanostructures and Nanodevices (CRANN) and Advanced Materials Bio-Engineering Research Centre (AMBER) and I-Form Research Centre, Trinity College Dublin, Dublin, Dublin 2, Ireland; Email: ji.liu@tcd.ie

Valeria Nicolosi − Centre for Research on Adaptive Nanostructures and Nanodevices (CRANN) and Advanced Materials Bio-Engineering Research Centre (AMBER), I-Form Research Centre, and School of Chemistry, Trinity College Dublin, Dublin, Dublin 2, Ireland; orcid.org/0000-0002-7637-4813; Email: nicolov@tcd.ie

Authors

Yunyi Zhu − College of Materials Science and Engineering, Hunan University, Changsha, Hunan 410082, China

Tong Guo − School of Aeronautics and Astronautics, Central South University, Changsha, Hunan 410083, China

Jing Jing Wang − Centre for Research on Adaptive Nanostructures and Nanodevices (CRANN) and Advanced Materials Bio-Engineering Research Centre (AMBER), Trinity College Dublin, Dublin, Dublin 2, Ireland

Xiuzhi Tang − School of Aeronautics and Astronautics, Central South University, Changsha, Hunan 410083, China

Complete contact information is available at: https://pubs.acs.org/10.1021/acsnano.0c08830

Notes

The authors declare no competing financial interest.

ACKNOWLEDGMENTS

We acknowledge the financial support from the National Natural Science Foundation of China (51703248), the Natural Science Foundation of Hunan Province (2019JJ50033), the
Fundamental Research Funds for the Central Universities, the
Science Foundation Ireland (SFI) AMBER Centre, and the European Research Council (ERC) CoG 3D2DPrint and PoC eTextiles.

REFERENCES

(1) Akyildiz, I. F.; Jornet, J. M.; Han, C. Terahertz Band: Next Frontier for Wireless Communications. Phys. Commun. 2014, 12, 16− 32.

(2) Nagatsuma, T.; Ducournau, G.; Renaud, C. C. Advances in Terahertz Communications Accelerated by Photonics. Nat. Photonics 2016, 10, 371−379.

(3) Ferguson, B.; Zhang, X.-C. Materials for Terahertz Science and Technology. Nat. Mater. 2002, 1, 26−33.

(4) Watts, C. M.; Shrekenhamer, D.; Montoya, J.; Lipworth, G.; Hunt, J.; Sleasman, T.; Krishna, S.; Smith, D. R.; Padilla, W. J. Terahertz Compressive Imaging with Metamaterial Spatial Light Modulators. Nat. Photonics 2014, 8, 605−609.

(5) Tonouchi, M. Cutting-Edge Terahertz Technology. Nat. Photonics 2007, 1, 97−105.

(6) Stantchev, R. I.; Sun, B.; Hornett, S. M.; Hobson, P. A.; Gibson, G. M.; Padgett, M. J.; Hendry, E. Noninvasive, Near-Field Terahertz Imaging of Hidden Objects Using a Single-Pixel Detector. Sci. Adv. 2016, 2, No. e1600190.

(7) Li, G.; Amer, N.; Hafez, H. A.; Huang, S.; Turchinovich, D.; Mochalin, V. N.; Hegmann, F. A.; Titova, L. V. Dynamical Control over Terahertz Electromagnetic Interference Shielding with 2D $Ti_3C_2T_y$ MXene by Ultrafast Optical Pulses. Nano Lett. 2020, 20, 636−643.

(8) Chen, H.; Ma, W.; Huang, Z.; Zhang, Y.; Huang, Y.; Chen, Y. Graphene-Based Materials toward Microwave and Terahertz Absorbing Stealth Technologies. Adv. Opt. Mater. 2019, 7, 1801318.

(9) Al-Saleh, M. H.; Sundararaj, U. Electromagnetic Interference Shielding Mechanisms of CNT/Polymer Composites. Carbon 2009, 47, 1738−1746.

(10) Shahzad, F.; Alhabeb, M.; Hatter, C. B.; Anasori, B.; Man Hong, S.; Koo, C. M.; Gogotsi, Y. Electromagnetic Interference Shielding with 2D Transition Metal Carbides (MXenes). Science 2016, 353, 1137−1140.

(11) Liu, L.; Das, A.; Megaridis, C. M. Terahertz Shielding of Carbon Nanomaterials and Their Composites-A Review and Applications. Carbon 2014, 69, 1−16.

(12) Liu, J.; Liu, Y.; Zhang, H.-B.; Dai, Y.; Liu, Z.; Yu, Z.-Z. Superelastic and Multifunctional Graphene-Based Aerogels by Interfacial Reinforcement with Graphitized Carbon at High Temperatures. Carbon 2018, 132, 95−103.

(13) Wei, Q.; Pei, S.; Qian, X.; Liu, H.; Liu, Z.; Zhang, W.; Zhou, T.; Zhang, Z.; Zhang, X.; Cheng, H.-M.; Ren, W. Superhigh Electromagnetic Interference Shielding of Ultrathin Aligned Pristine Graphene Nanosheets Film. Adv. Mater. 2020, 32, 1907411.

(14) Zhang, J.; Kong, N.; Uzun, S.; Levitt, A.; Seyedin, S.; Lynch, P. A.; Qin, S.; Han, M.; Yang, W.; Liu, J.; Wang, X.; Gogotsi, Y.; Razal, J. M. Scalable Manufacturing of Free-Standing, Strong $Ti_3C_2T_x$ MXene Films with Outstanding Conductivity. Adv. Mater. 2020, 32, 2001093.

(15) Yao, B.; Hong, W.; Chen, T.; Han, Z.; Xu, X.; Hu, R.; Hao, J.; Li, C.; Li, H.; Perini, S. E.; Lanagan, M. T.; Zhang, S.; Wang, Q.; Wang, H. Highly Stretchable Polymer Composite with StrainEnhanced Electromagnetic Interference Shielding Effectiveness. Adv. Mater. 2020, 32, 1907499.

(16) Zhou, E.; Xi, J.; Liu, Y.; Xu, Z.; Guo, Y.; Peng, L.; Gao, W.; Ying, J.; Chen, Z.; Gao, C. Large-Area Potassium-Doped Highly Conductive Graphene Films for Electromagnetic Interference Shielding. Nanoscale 2017, 9, 18613−18618.

(17) Wan, S.; Chen, Y.; Wang, Y.; Li, G.; Wang, G.; Liu, L.; Zhang, J.; Liu, Y.; Xu, Z.; Tomsia, A. P.; Jiang, L.; Cheng, Q. Ultrastrong Graphene Films via Long-Chain π-Bridging. Matter 2019, 1, 389− 401.

(18) Shen, B.; Zhai, W.; Zheng, W. Ultrathin Flexible Graphene Film: An Excellent Thermal Conducting Material with Efficient EMI Shielding. Adv. Funct. Mater. 2014, 24, 4542−4548.

(19) Sun, R.; Zhang, H.-B.; Liu, J.; Xie, X.; Yang, R.; Li, Y.; Hong, S.; Yu, Z.-Z. Highly Conductive Transition Metal Carbide/Carbonitride(MXene)@Polystyrene Nanocomposites Fabricated by Electrostatic Assembly for Highly Efficient Electromagnetic Interference Shielding. Adv. Funct. Mater. 2017, 27, 1702807.

(20) Zhou, Y.; E, Y.; Zhu, L.; Qi, M.; Xu, X.; Bai, J.; Ren, Z.; Wang, L. Terahertz Wave Reflection Impedance Matching Properties of Graphene Layers at Oblique Incidence. Carbon 2016, 96, 1129−1137.

(21) Micheli, D.; Vricella, A.; Pastore, R.; Marchetti, M. Synthesis and Electromagnetic Characterization of Frequency Selective Radar Absorbing Materials Using Carbon Nanopowders. Carbon 2014, 77, 756−774.

(22) Zhang, Y.; Huang, Y.; Zhang, T.; Chang, H.; Xiao, P.; Chen, H.; Huang, Z.; Chen, Y. Broadband and Tunable High-Performance Microwave Absorption of an Ultralight and Highly Compressible Graphene Foam. Adv. Mater. 2015, 27, 2049−2053.

(23) Li, X.; Yin, X.; Song, C.; Han, M.; Xu, H.; Duan, W.; Cheng, L.; Zhang, L. Self-Assembly Core-Shell Graphene-Bridged Hollow MXenes Spheres 3D Foam with Ultrahigh Specific EM Absorption Performance. Adv. Funct. Mater. 2018, 28, 1803938.

(24) Mahmoodi, M.; Arjmand, M.; Sundararaj, U.; Park, S. The Electrical Conductivity and Electromagnetic Interference Shielding of Injection Molded Multi-Walled Carbon Nanotube/Polystyrene Composites. Carbon 2012, 50, 1455−1464.

(25) Zhu, H.-F.; Du, L.-H.; Li, J.; Shi, Q.-W.; Peng, B.; Li, Z.-R.; Huang, W.-X.; Zhu, L.-G. Near-Perfect Terahertz Wave Amplitude Modulation Enabled by Impedance Matching in VO_2 Thin Films. Appl. Phys. Lett. 2018, 112, 081103.

(26) Zeng, Z.; Jin, H.; Chen, M.; Li, W.; Zhou, L.; Zhang, Z. Lightweight and Anisotropic Porous MWCNT/WPU Composites for Ultrahigh Performance Electromagnetic Interference Shielding. Adv. Funct. Mater. 2016, 26, 303−310.

(27) Song, Q.; Ye, F.; Yin, X.; Li, W.; Li, H.; Liu, Y.; Li, K.; Xie, K.; Li, X.; Fu, Q.; Cheng, L.; Zhang, L.; Wei, B. Carbon NanotubeMultilayered Graphene Edge Plane Core-Shell Hybrid Foams for Ultrahigh-Performance Electromagnetic-Interference Shielding. Adv. Mater. 2017, 29, 1701583.

(28) Han, M.; Yin, X.; Hantanasirisakul, K.; Li, X.; Iqbal, A.; Hatter, C. B.; Anasori, B.; Koo, C. M.; Torita, T.; Soda, Y.; Zhang,

L.; Cheng, L.; Gogotsi, Y. Anisotropic MXene Aerogels with a Mechanically Tunable Ratio of Electromagnetic Wave Reflection to Absorption. Adv. Opt. Mater. 2019, 7, 1900267.

(29) Liu, J.; Zhang, H.-B.; Sun, R.; Liu, Y.; Liu, Z.; Zhou, A.; Yu, Z.Z. Hydrophobic, Flexible, and Lightweight MXene Foams for HighPerformance Electromagnetic-Interference Shielding. Adv. Mater. 2017, 29, 1702367.

(30) Shui, W.; Li, J.; Wang, H.; Xing, Y.; Li, Y.; Yang, Q.; Xiao, X.; Wen, Q.; Zhang, H. $Ti_3C_2T_x$ MXene Sponge Composite as

Broadband Terahertz Absorber. Adv. Opt. Mater. 2020, 8, 2001120.

(31) Li, Y.; Lan, X.; Wu, F.; Liu, J.; Huang, P.; Chong, Y.; Luo, H.; Shen, B.; Zheng, W. Steam-Chest Molding of Polypropylene/Carbon Black Composite Foams as Broadband EMI Shields with High Absorptivity. Compos. Commun. 2020, 22, 100508.

(32) Lin, Z.; Liu, J.; Peng, W.; Zhu, Y.; Zhao, Y.; Jiang, K.; Peng, M.; Tan, Y. Highly Stable 3D $Ti_3C_2T_x$ MXene-Based Foam Architectures toward High-Performance Terahertz Radiation Shielding. ACS Nano 2020, 14, 2109−2117.

(33) Chen, Z.; Xu, C.; Ma, C.; Ren, W.; Cheng, H.-M. Lightweight and Flexible Graphene Foam Composites for High-Performance Electromagnetic Interference Shielding. Adv. Mater. 2013, 25, 1296− 1300.

(34) King, G. W.; Hainer, R. M.; Cross, P. C. Expected Microwave Absorption Coefficients of Water and Related Molecules. Phys. Rev. 1947, 71, 433−443.

(35) van Vleck, J. H. The Absorption of Microwaves by Uncondensed Water Vapor. Phys. Rev. 1947, 71, 425−433.

(36) Hogg, D. C.; Guiraud, F. O. Microwave Measurements of the Absolute Values of Absorption by Water Vapour in the Atmosphere. Nature 1979, 279, 408−409.

(37) Garner, H. R.; Ohkawa, T.; Tuason, O.; Lee, R. L. Microwave Absorption in Substances That Form Hydration Layers with Water. Phys. Rev. A: At., Mol., Opt. Phys. 1990, 42, 7264−7270.

(38) Song, W.-L.; Zhang, Y.-J.; Zhang, K.-L.; Wang, K.; Zhang, L.; Chen, L.-L.; Huang, Y.; Chen, M.; Lei, H.; Chen, H.; Fang, D. Ionic Conductive Gels for Optically Manipulatable Microwave Stealth Structures. Adv. Sci. 2020, 7, 1902162.

(39) Zhang, Y. S.; Khademhosseini, A. Advances in Engineering Hydrogels. Science 2017, 356, No. eaaf3627.

(40) Sun, S.; Mao, L.-B.; Lei, Z.; Yu, S.-H.; Cölfen, H. Hydrogels from Amorphous Calcium Carbonate and Polyacrylic Acid: BioInspired Materials for “Mineral Plastics. Angew. Chem., Int. Ed. 2016, 55, 11765−11769.

(41) Lei, Z.; Wu, P. A Highly Transparent and Ultra-Stretchable Conductor with Stable Conductivity during Large Deformation. Nat. Commun. 2019, 10, 3429.

(42) Jiang, Z.; Diggle, B.; Shackleford, I. C. G.; Connal, L. A. Tough, Self-Healing Hydrogels Capable of Ultrafast Shape Changing. Adv. Mater. 2019, 31, 1904956.

(43) Iqbal, A.; Shahzad, F.; Hantanasirisakul, K.; Kim, M.-K.; Kwon, J.; Hong, J.; Kim, H.; Kim, D.; Gogotsi, Y.; Koo, C. M. Anomalous Absorption of Electromagnetic Waves by 2D Transition Metal Carbonitride (MXene). Science. 2020, 369, 446−450.

(44) Yun, T.; Kim, H.; Iqbal, A.; Cho, Y. S.; Lee, G. S.; Kim, M.-K.; Kim, S. J.; Kim, D.; Gogotsi, Y.; Kim, S. O.; Koo, C. M. Electromagnetic Shielding of Monolayer MXene Assemblies. Adv. Mater. 2020, 32, 1906769.

(45) Wang, Q.-W.; Zhang, H.-B.; Liu, J.; Zhao, S.; Xie, X.; Liu, L.; Yang, R.; Koratkar, N.; Yu, Z.-Z. Multifunctional and Water-Resistant MXene-Decorated Polyester Textiles with Outstanding Electromagnetic Interference Shielding and Joule Heating Performances. Adv. Funct. Mater. 2019, 29, 1806819.

(46) Cao, W.-T.; Chen, F.-F.; Zhu, Y.-J.; Zhang, Y.-G.; Jiang, Y.-Y.; Ma, M.-G.; Chen, F. Binary Strengthening and Toughening of MXene/Cellulose Nanofiber Composite Paper with Nacre-Inspired Structure and Superior Electromagnetic Interference Shielding Properties. ACS Nano 2018, 12, 4583−4593.

(47) Han, M.; Shuck, C. E.; Rakhmanov, R.; Parchment, D.; Anasori, B.; Koo, C. M.; Friedman, G.; Gogotsi, Y. Beyond $Ti_3C_2T_x$: MXenes for Electromagnetic Interference Shielding. ACS Nano 2020, 14, 5008−5016.

(48) Chen, W.; Liu, L.-X.; Zhang, H.-B.; Yu, Z.-Z. Flexible, Transparent, and Conductive $Ti_3C_2T_x$ MXene-Silver Nanowire Films with Smart Acoustic Sensitivity for High-Performance Electromagnetic Interference Shielding. ACS Nano 2020, 14, 16643−16653. (49) Choi, G.; Shahzad, F.; Bahk, Y.-M.; Jhon, Y. M.; Park, H.; Alhabeb, M.; Anasori, B.; Kim, D.-S.; Koo, C. M.; Gogotsi, Y.; Seo, M. Enhanced Terahertz Shielding of MXenes with Nano-Metamaterials. Adv. Opt. Mater. 2018, 6, 1701076.

(50) Cao, M.-S.; Cai, Y.-Z.; He, P.; Shu, J.-C.; Cao, W.-Q.; Yuan, J. 2D MXenes: Electromagnetic Property for Microwave Absorption and Electromagnetic Interference Shielding. Chem. Eng. J. 2019, 359, 1265−1302.

(51) Zhang, J.; Uzun, S.; Seyedin, S.; Lynch, P. A.; Akuzum, B.; Wang, Z.; Qin, S.; Alhabeb, M.; Shuck, C. E.; Lei, W.; Kumbur, E. C.; Yang, W.; Wang, X.; Dion, G.; Razal, J. M.; Gogotsi, Y. Additive-Free MXene Liquid Crystals and Fibers. ACS Cent. Sci. 2020, 6, 254−265.

(52) Ling, Z.; Ren, C. E.; Zhao, M.-Q.; Yang, J.; Giammarco, J. M.; Qiu, J.; Barsoum, M. W.; Gogotsi, Y. Flexible and Conductive MXene Films and Nanocomposites with High Capacitance. Proc. Natl. Acad. Sci. U. S. A. 2014, 111, 16676−16681.

(53) Wu, Z.; Shang, T.; Deng, Y.; Tao, Y.; Yang, Q.-H. The Assembly of MXenes from 2D to 3D. Adv. Sci. 2020, 7, 1903077.

(54) Liu, J.; Zhang, H.-B.; Xie, X.; Yang, R.; Liu, Z.; Liu, Y.; Yu, Z.-Z. Multifunctional, Superelastic, and Lightweight MXene/Polyimide Aerogels. Small 2018, 14, 1802479.

(55) Lin, S.; Zhong, Y.; Zhao, X.; Sawada, T.; Li, X.; Lei, W.; Wang, M.; Serizawa, T.; Zhu, H. Synthetic Multifunctional Graphene Composites with Reshaping and Self-Healing Features via a Facile Biomineralization-Inspired Process. Adv. Mater. 2018, 30, 1803004.

(56) Alhabeb, M.; Maleski, K.; Anasori, B.; Lelyukh, P.; Clark, L.; Sin, S.; Gogotsi, Y. Guidelines for Synthesis and Processing of TwoDimensional Titanium Carbide ($Ti_3C_2T_x$ MXene). Chem. Mater. 2017, 29, 7633−7644.

(57) Zhou, T.; Wu, C.; Wang, Y.; Tomsia, A. P.; Li, M.; Saiz, E.; Fang, S.; Baughman, R. H.; Jiang, L.; Cheng, Q. Super-Tough MXeneFunctionalized Graphene Sheets. Nat. Commun. 2020, 11, 2077.

(58) Feig, V. R.; Tran, H.; Lee, M.; Bao, Z. Mechanically Tunable Conductive Interpenetrating Network Hydrogels That Mimic the Elastic Moduli of Biological Tissue. Nat. Commun. 2018, 9, 2740.

(59) Sun, J.-Y.; Zhao, X.; Illeperuma, W. R. K.; Chaudhuri, O.; Oh, K. H.; Mooney, D. J.; Vlassak, J. J.; Suo, Z. Highly Stretchable and Tough Hydrogels. Nature 2012, 489, 133−136.
(60) Cheng, H.; Huang, Y.; Cheng, Q.; Shi, G.; Jiang, L.; Qu, L. SelfHealing Graphene Oxide Based Functional Architectures Triggered by Moisture. Adv. Funct. Mater. 2017, 27, 1703096.
(61) Huang, Z.; Chen, H.; Huang, Y.; Ge, Z.; Zhou, Y.; Yang, Y.; Xiao, P.; Liang, J.; Zhang, T.; Shi, Q.; Li, G.; Chen, Y. UltraBroadband Wide-Angle Terahertz Absorption Properties of 3D Graphene Foam. Adv. Funct. Mater. 2018, 28, 1704363.
(62) Yousefi, N.; Sun, X.; Lin, X.; Shen, X.; Jia, J.; Zhang, B.; Tang, B.; Chan, M.; Kim, J.-K. Highly Aligned Graphene/Polymer Nanocomposites with Excellent Dielectric Properties for HighPerformance Electromagnetic Interference Shielding. Adv. Mater. 2014, 26, 5480−5487.
(63) Zhao, J.; Wei, S.; Wang, C.; Chen, K.; Zhu, B.; Jiang, T.; Feng, Y. Broadband Microwave Absorption Utilizing Water-Based Metamaterial Structures. Opt. Express 2018, 26, 8522−8531.
(64) Zhang, Y.-Z.; Lee, K. H.; Anjum, D. H.; Sougrat, R.; Jiang, Q.; Kim, H.; Alshareef, H. N. MXenes Stretch Hydrogel Sensor Performance to New Limits. Sci. Adv. 2018, 4, No. eaat0098.
(65) Xu, C.; Yang, Y.; Gao, W. Skin-Interfaced Sensors in Digital Medicine: From Materials to Applications. Matter 2020, 2, 1414− 1445.